ATLAS Internal Note
INDET-No-139
September 3, 1996

Determination of Leakage Currents and Depletion Voltages of Pixel Test Structures

Grant Gorfine and Sally Seidel

New Mexico Center for Particle Physics
University of New Mexico
Albuquerque, New Mexico 87131 U.S.A.

Steve Holland

Lawrence Berkeley National Laboratory
University of California
Berkeley, California 94720 U.S.A.

Abstract

Leakage currents of unirradiated and irradiated silicon test structures were measured. The irradiated structures received the equivalent of 4.8×10^{13} cm^{-2} 1 MeV neutrons. Damage coefficients were calculated (with corrections made for annealing) and compared with published values to determine whether the currents measured in the structures under test were ascribable to known damage mechanisms. A peak in curves of current versus voltage was observed for irradiated n-type detectors which had inverted. The relationship between the peak and the voltage of full depletion was examined. In p-type detectors, significant diminishment of the breakdown voltage with irradiation was observed.

1 Introduction and Description of the Test Structures

Leakage currents were measured on unirradiated and irradiated silicon test structures. These test structures were fabricated at LBNL in 1994 in both n-type and p-type.

The layout of the structures on the radiation test device is shown in Fig. 1. The structures for which measurements have been made are a 6.7×3.2 mm^2 diode, a 2 mm^2 diode, a 1 mm^2 diode, a 330×330 μm^2 diode, a 450×75 μm^2 diode, and six 3×9 arrays of pixels whose dimensions are described below. The thickness of the detectors is 300 μm.

Fig. 2 shows the details of one pixel array. The center pixel is isolated while the surrounding pixels are connected together. This allows all the surrounding pixels to be biased with a single probe. The pitch is 50 μm in the y direction and 536 μm in the x direction. For the p-type detectors there is a p^+ isolation implant (sometimes referred to as a "p-stop") surrounding the n^+ implants. The widths of the pixel implants (p^+ in the case of n-type bulk and n^+ in the case of p-type bulk) vary for each array. For the p-type detectors the p-stop widths and the gap between the n^+ implants and p-stops also vary in the six arrays. The pixel implant width is denoted W, and the p-stop width is denoted P. The gap between the p-stop and the n^+ implant is the same as the p-stop width except in Array 4, which had a layout error. The values for W and P of the six arrays are given in Table 1.

2 Overview of Measurements, Irradiation, and Temperature History

Table 2 summarizes the detectors which have been measured and the labels used to identify them. The two unirradiated detectors were unmounted and were measured using a probe station. Irradiated detectors were mounted prior to irradiation on G10 circuit boards. Two boards were placed in the beam as shown in Fig. 3. The board labeled "C" was upstream and had two p-type detectors, "pcm" and "pcr", mounted on it. Only results from detector "pcm" are presented. The board labeled "A" had two n-type detectors, "nam" and "nar" mounted on it. Results for both these detectors are presented. The detectors mounted on boards had the 6.7×3.2 mm^2 diode, the 2 mm^2 diode, and the 1 mm^2 diode wire bonded to traces leading to connectors so that electrical measurements could be made of these structures without probing. The remaining diodes were probed directly. The mounting of the detectors on boards is not expected to have a significant effect on the results shown in this report.

Detectors were irradiated with 55 MeV protons at the 88" Cyclotron at LBNL. The beam fluence was 2.6×10^{13} (55 MeV p)/cm^2 as measured by an ionization chamber. The equivalent 1 MeV neutron fluence was calculated by taking the non-ionizing

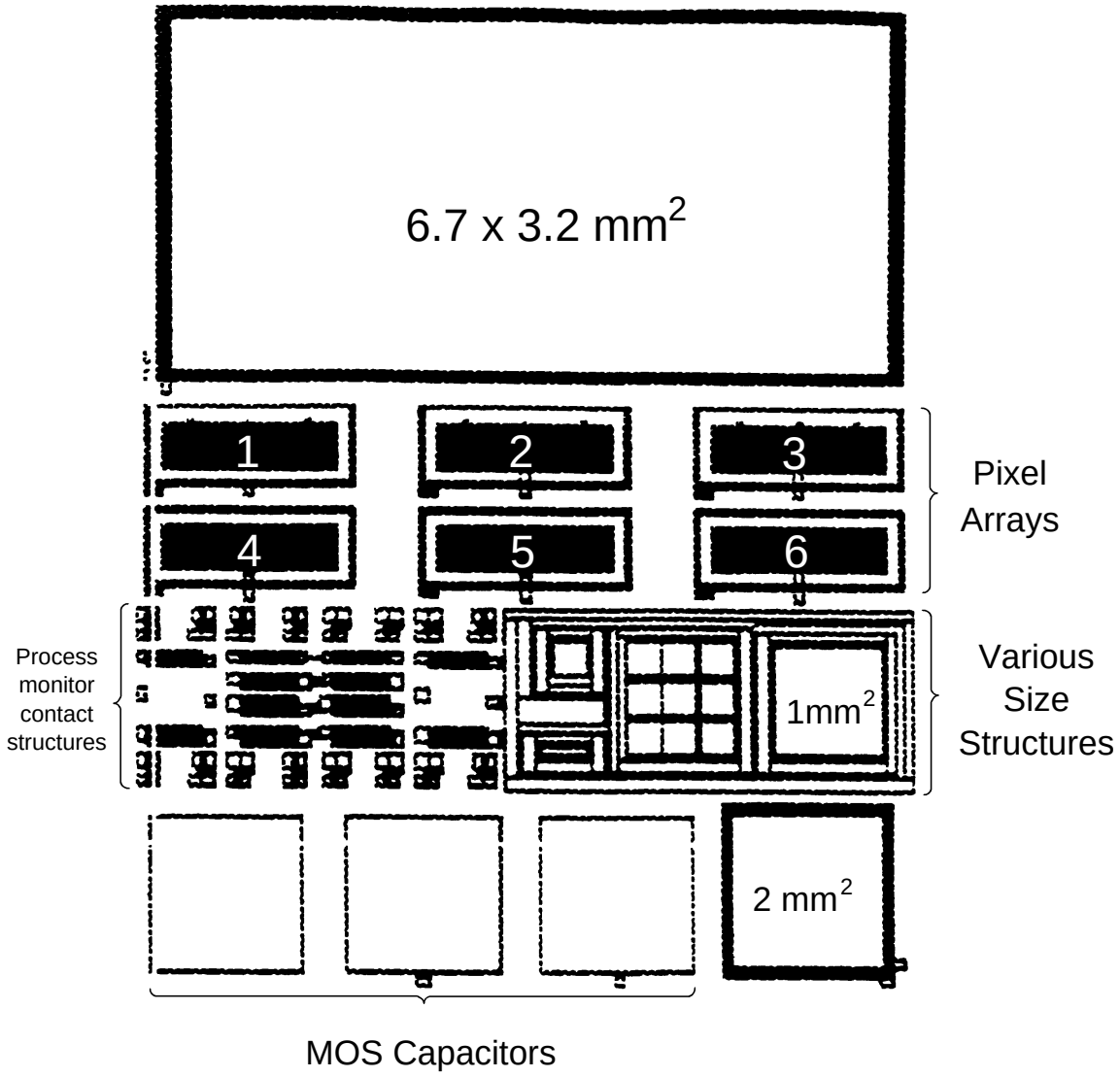

Figure 1: Diagram of the LBNL radiation damage test chip. The six "Pixel Arrays" are each a 3×9 array of pixels. Fig. 2 shows the detail of one pixel array. The region labeled "Various Size Structures" contains a 1 mm^2 diode as indicated, a 330×330 $\mu\mathrm{m}^2$ diode in the upper left corner, a 450×75 $\mu\mathrm{m}^2$ diode in the lower left corner, and a 3×3 array of 330×330 $\mu\mathrm{m}^2$ diodes in the middle.

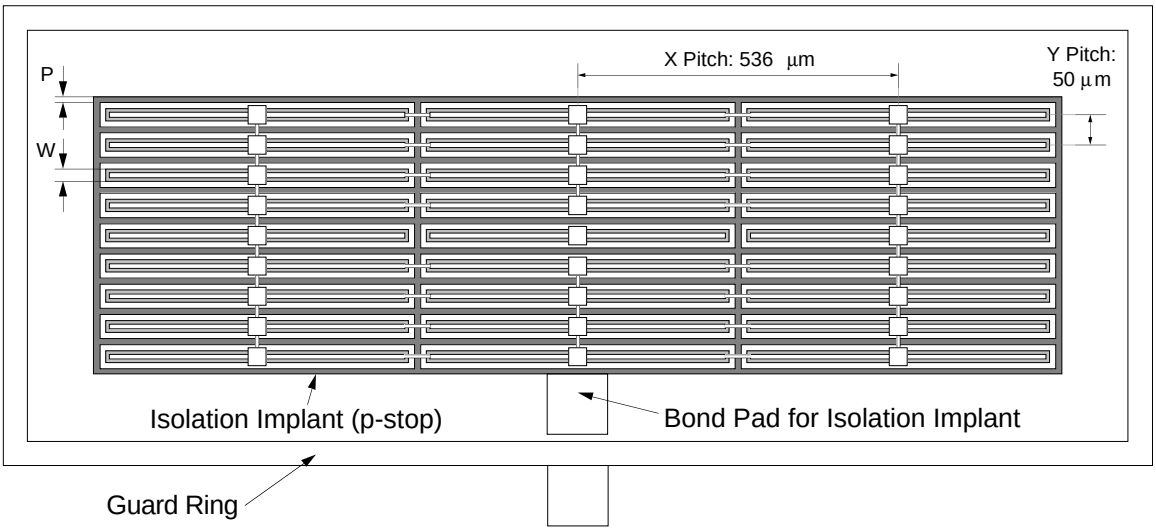

Figure 2: Diagram of a p-type pixel array. A p^+ isolation implant surrounds the pixels. The n-type detectors look similar but lack an isolation implant. The isolation implant width is denoted P, and the pixel implant width is denoted W.

Table 1 Summary of the dimensions of the pixel arrays. See text for definitions of W and P.

Pixel Array No.	W (μm)	P (μm)
1	20	0
2	38	4
3	32	6
4	23	8
5	20	10
6	14	12

Note: In Array 4 ($W = 23, P = 8$) there was an error in the layout which caused the gap to be 8 μm wide on one side and 11 μm wide on the other.

Table 2 Summary of detectors measured and the labels used to identify them.

Description	Detector Label
Unirradiated n-type	n1
Unirradiated p-type	p1
Board A n-type Middle Detector	nam
Board A n-type Right Detector	nar
Board C p-type Middle Detector	pcm

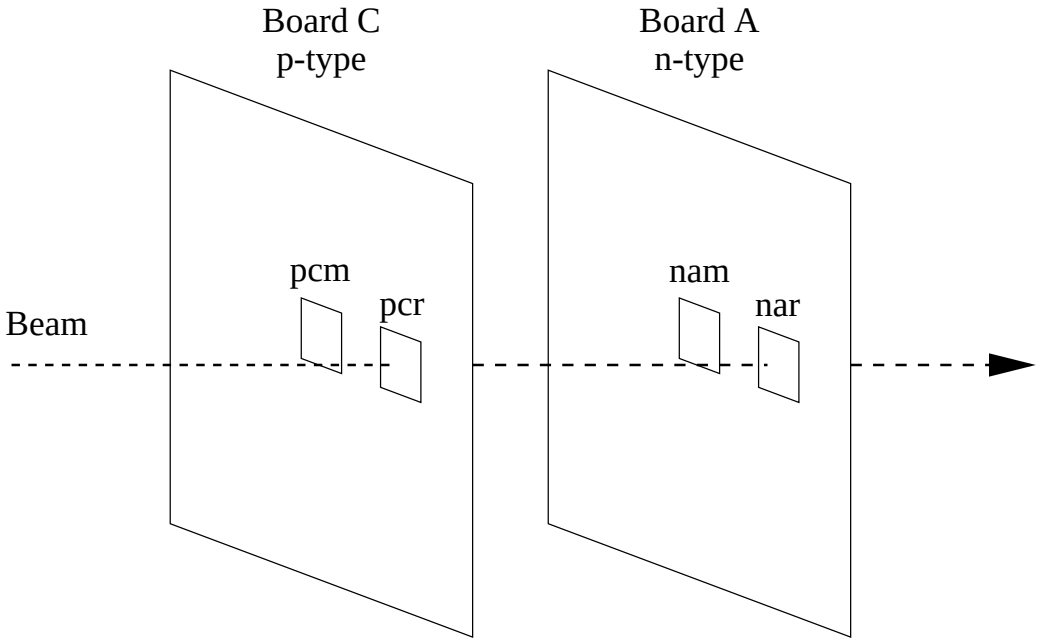

Figure 3: Schematic diagram of the position of boards and detectors in the beam. The beam spot is likely to have been positioned approximately as shown as inferred from variations in the measured leakage currents. The diagram is not to scale.

energy loss data for protons [1], converting to displacement damage (multiply by 46.5 MeV-mb/keV-cm^2-g^{-1}), and normalizing to 95 MeV-mb which is the ASTM [2] recommended value for the displacement damage of 1 MeV neutrons. The 55 MeV protons were calculated to be a factor 1.85 more damaging than 1 MeV neutrons and so the equivalent 1 MeV neutron fluence was 4.8×10^{13} cm^{-2}.

Observation of differences in the leakage currents of different structures on the test devices (to be discussed later) suggest that the beam profile was not uniform but rather was centered near detector "nar". The beam intensity appears to have varied across detector "nam".

Detectors were irradiated at room temperature and then stored at LBNL at -17°C. Detectors were warmed up briefly to room temperature during measurement. Although the detectors were shipped to UNM with dry ice, the dry ice sublimated completely during transport and so the time period during which detectors were warm (and therefore annealing) is not known. After transfer to UNM the detectors were stored at 0 ± 1°C. An estimate of the total time each detector spent at room temperature is 2 ± 1 days.

3 Leakage Current Results of n-type Detectors

3.1 Measurement of Leakage Currents

Measurements of current versus voltage ("I-V") were made on each test structure using a Keithley 237 as the bias supply and a Keithley 617 to measure the current. In all measurements of the pixel arrays, the surrounding pixels and guard ring were biased. The guard ring was also biased for the non-pixel (diode) measurements.

The temperature was monitored with a thermometer in close proximity to the probe station. Temperatures ranged from 22° to 25°C. Currents were normalized to 20°C with the following equation [3]:

$$I_{20} = I_T \left(\frac{293.2}{T + 273.2}\right)^2 \exp\left(-\frac{1.24}{2k_B}\left[\frac{1}{293.2} - \frac{1}{T + 273.2}\right]\right), \quad (1)$$

where k_B is Boltzmann's constant, I_T is the measured current, and T is the measured temperature in °C.

Figs. 4–7 show I-Vs for several n-type structures on detectors "nam" and "nar". An interesting feature is the peak that occurs at a few tens of volts. This behavior has also been observed by CPPM [4] who give as a possible explanation that the conductive region under the implants which exists prior to full depletion in an inverted detector is allowing current from regions other than directly beneath the implants to reach the implants. The high side of the peak may therefore be correlated with the point of full depletion. A similar effect has been observed in silicon microstrip sensors [5].

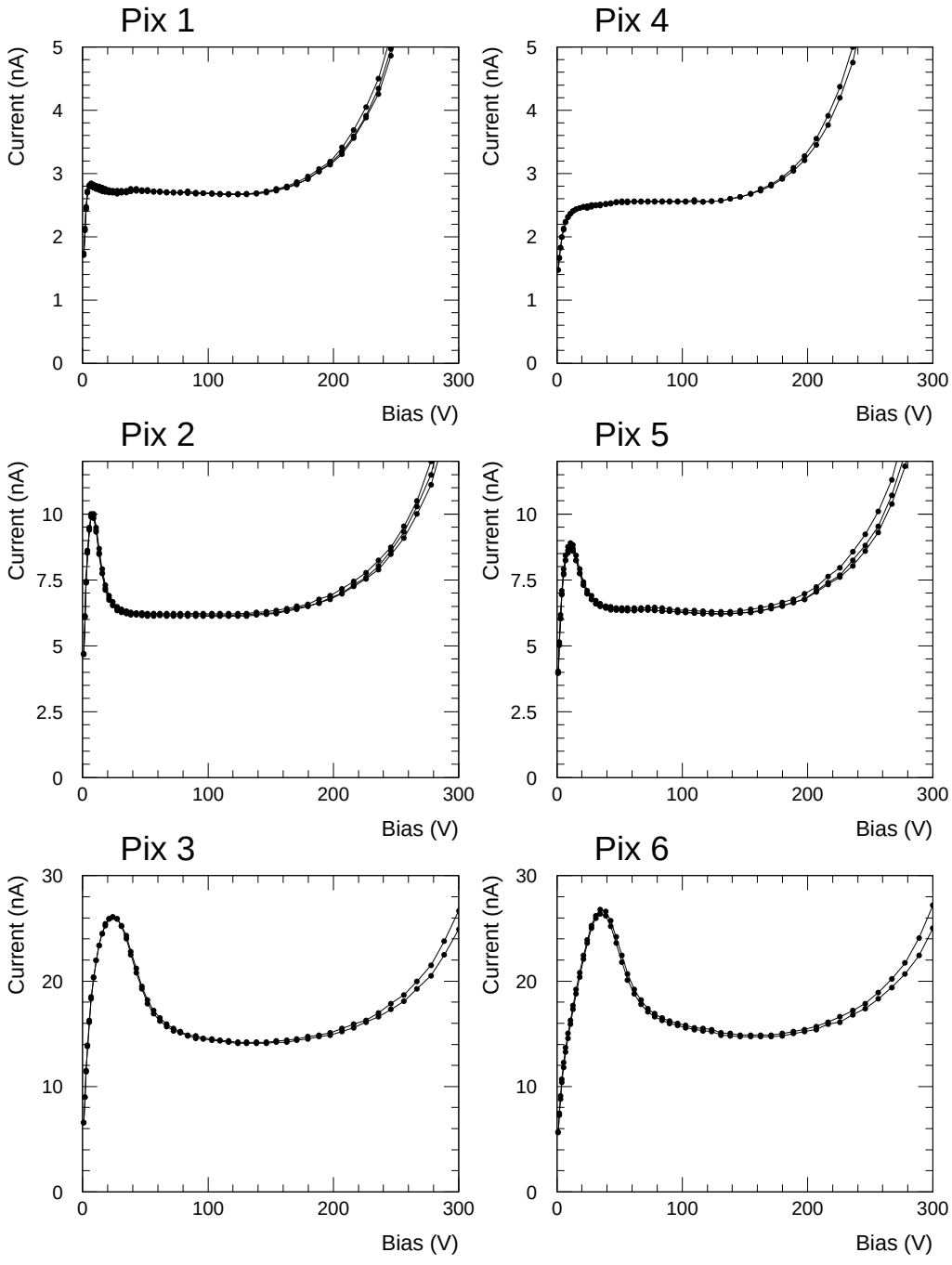

Figure 4: Currents in n-type pixel arrays on detector "nam". Currents were temperature corrected to 20°C. Multiple curves represent repeated measurements.

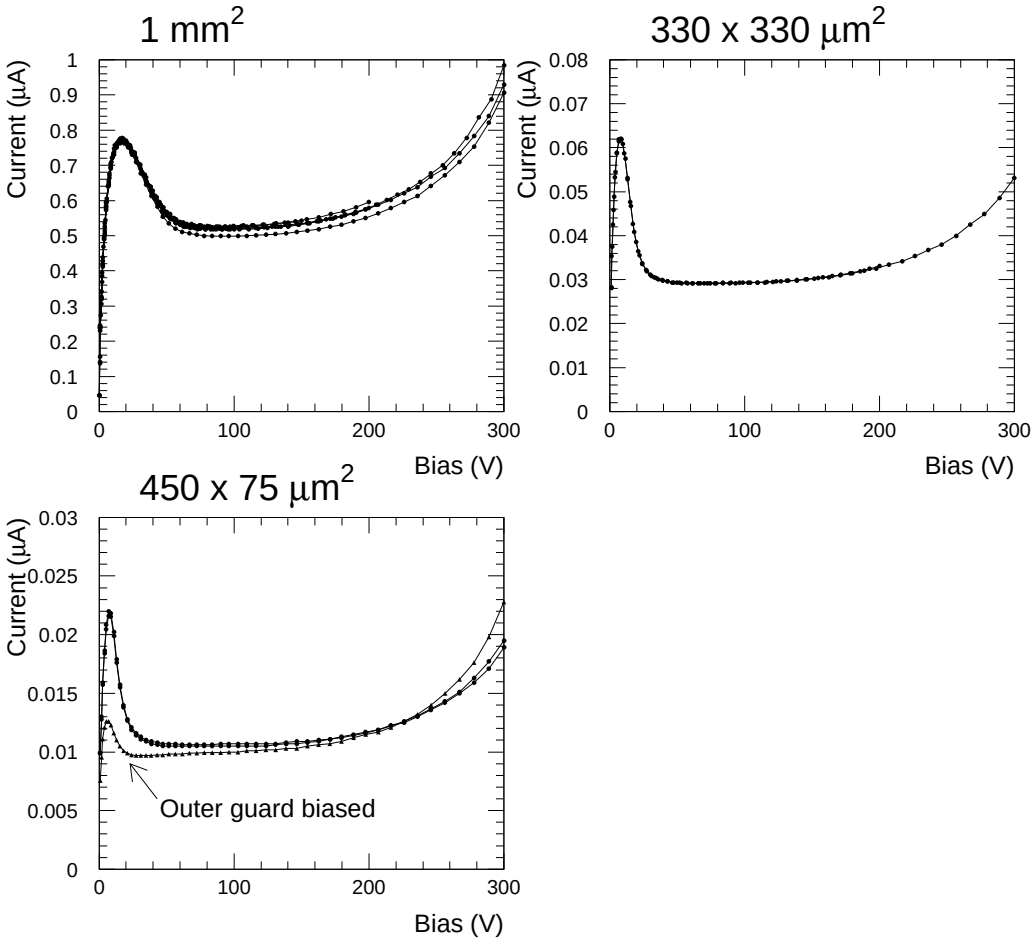

Figure 5: Currents in n-type non-pixel structures on detector "nam". Currents were temperature corrected to 20°C. Multiple curves represent repeated measurements. Triangular symbols indicate that the outer guard was biased (see text).

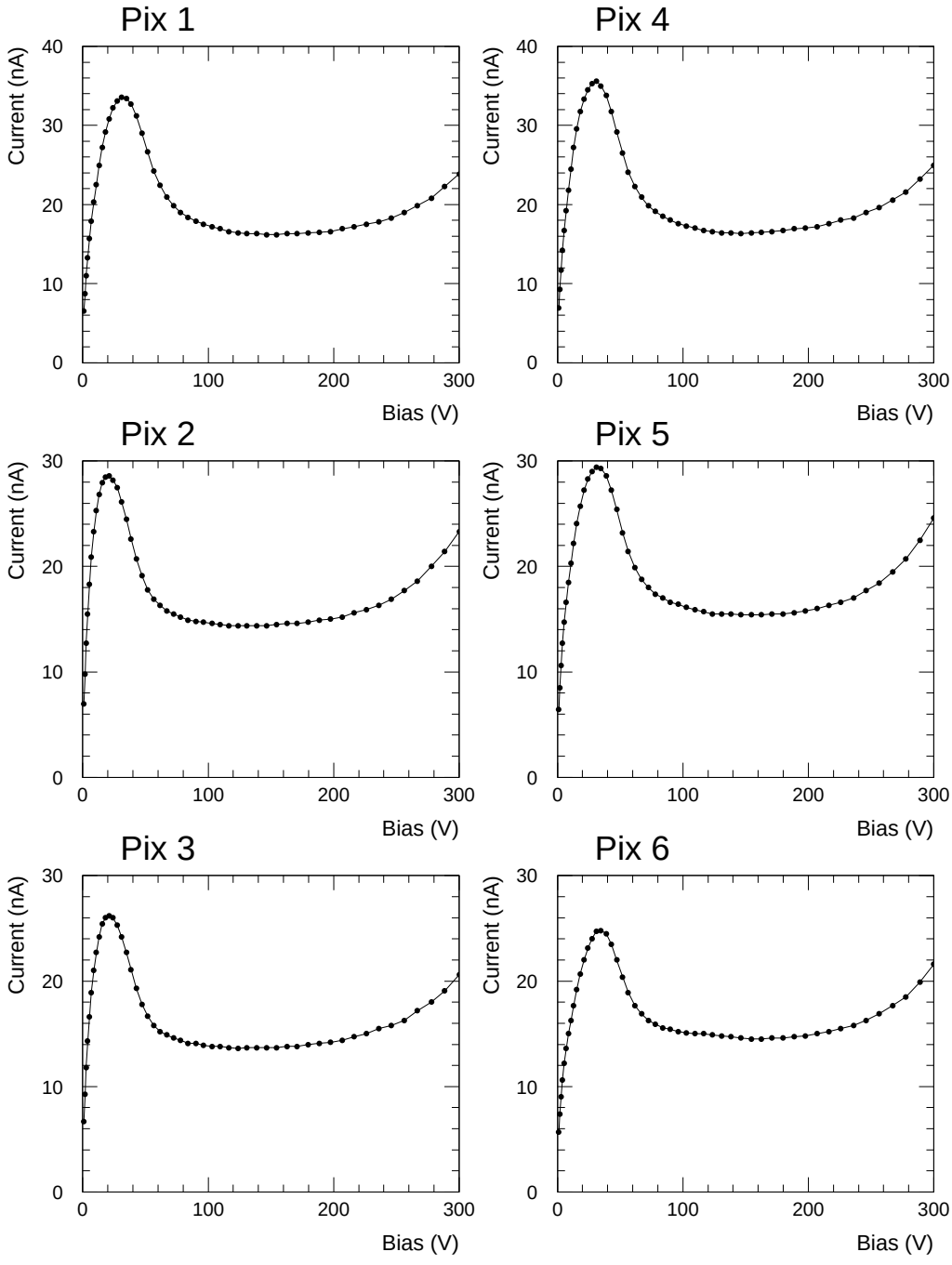

Figure 6: Currents in n-type pixel arrays on detector "nar". Currents were temperature corrected to 20°C.

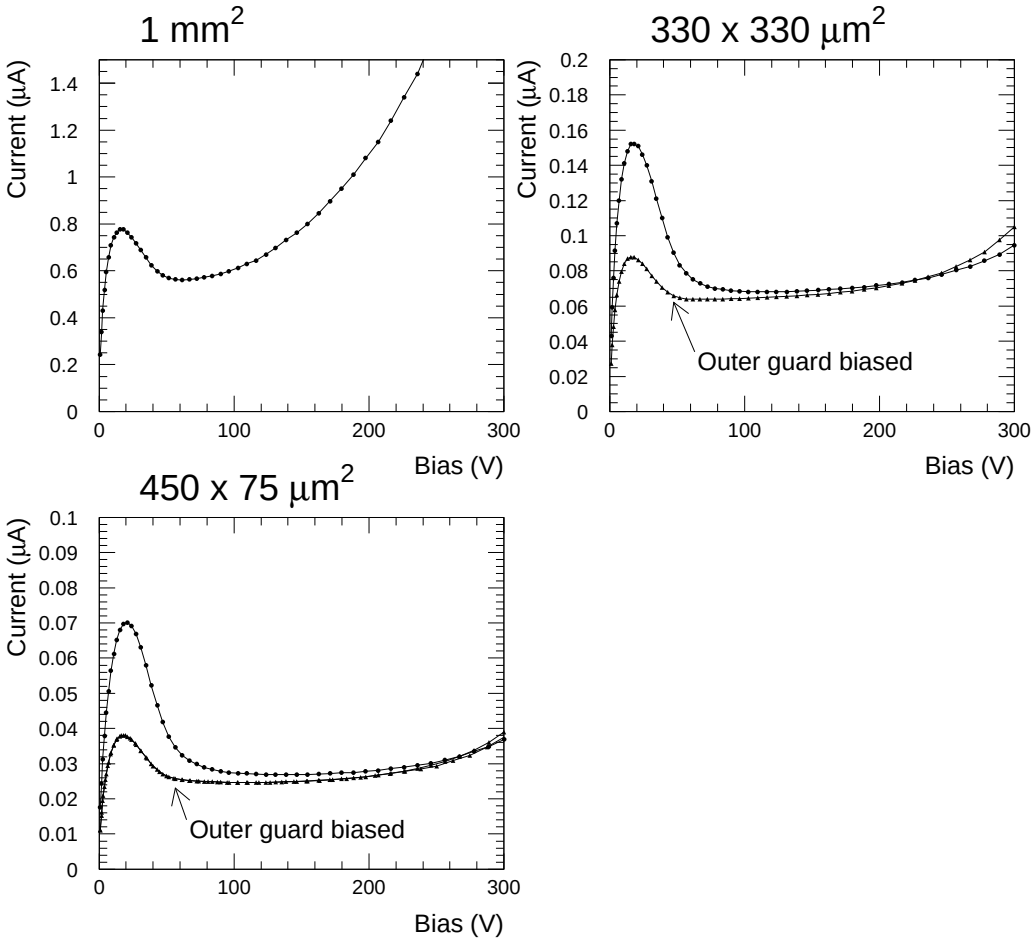

Figure 7: Currents in n-type non-pixel structures on detector "nar". Currents were temperature corrected to 20°C. Some structures were measured with and without the outer guard biased (see text).

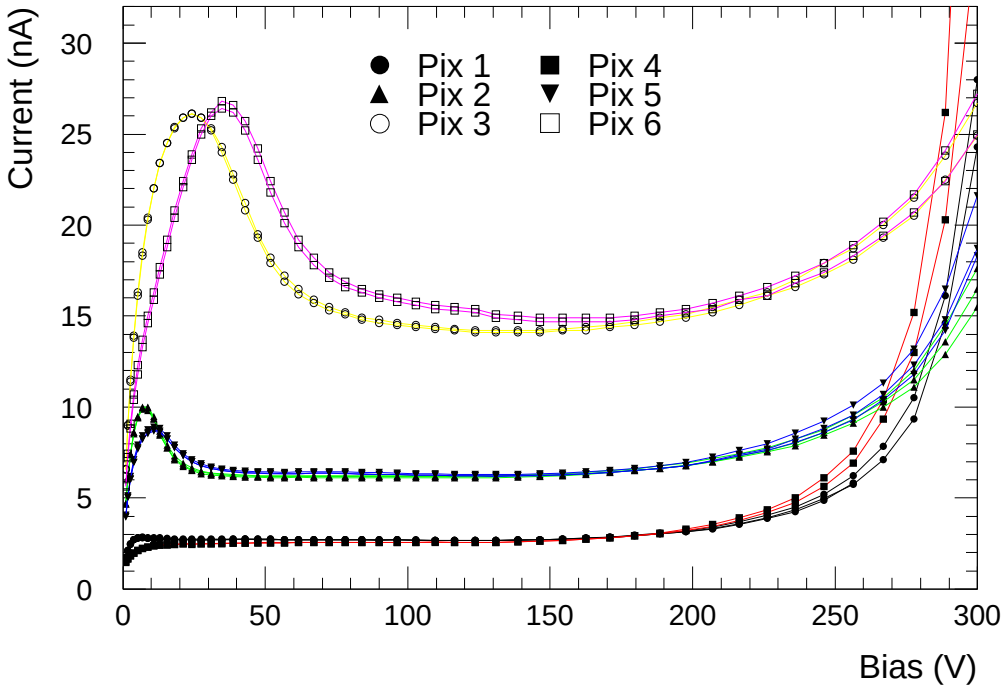

Figure 8: Leakage currents in all pixel arrays on detector "nam". Currents were temperature corrected to 20°C.

The 1 mm^2, 330 × 330 μm^2, and 450 × 75 μm^2 diodes are clustered together in the region labeled "various size structures" on Fig. 1. These "various size structures" have individual guard rings as well as a common implanted region (referred to as the outer guard) which surrounds them all. On a few of these structures measurements were made with and without the outer guard biased. With the outer guard biased, the height of the peak was less than it was with the outer guard unbiased. This is seen for the 450 × 75 μm^2 diode in Fig. 5 and for the 330 × 330 μm^2 and 450 × 75 μm^2 diodes in Fig. 7. A possible explanation is that with the outer guard biased, alternative paths are available to current generated in regions that are not directly beneath the implant.

Fig. 8 summarizes I-Vs for all the pixel structures on board "nam". The differences among the leakage current levels is consistent with these structures' being in a non-uniform region of the beam. Leakage current levels in detector "nar" are more uniform, as seen in Fig. 9. The profile of the beam which is implied by these variations in leakage current levels is discussed below.

For detector "nam" the pixels on the left (Pixels 1 & 4) are suspected to have

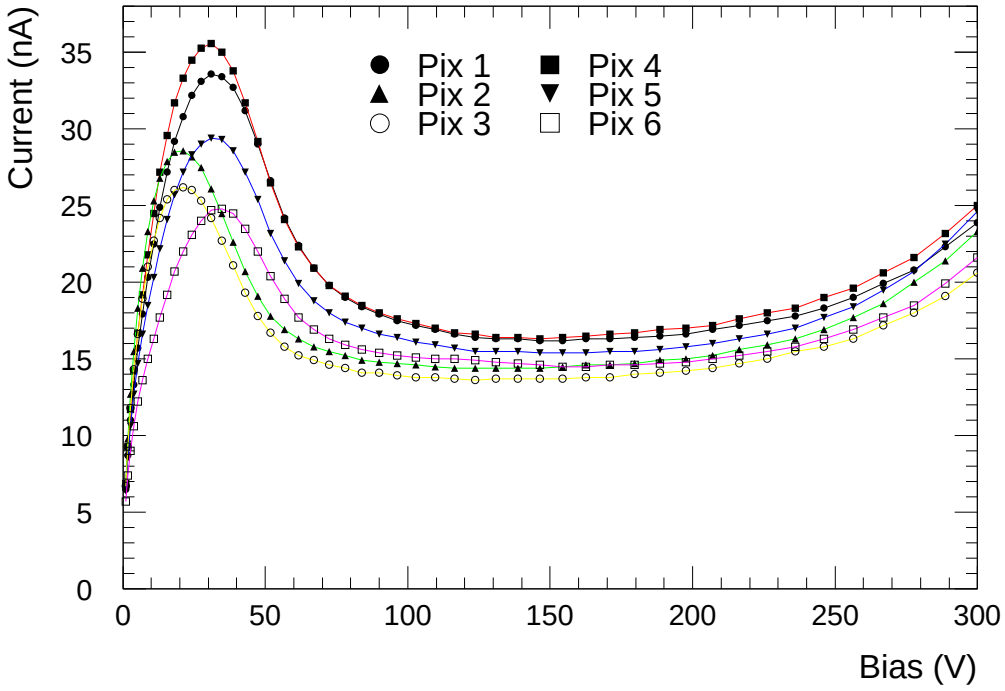

Figure 9: Leakage currents in all pixel arrays on detector "nar". Currents were temperature corrected to 20°C.

received the least fluence. The I-Vs for these two pixel arrays showed little or no current peak. The explanation proposed above for the cause of the peaks requires the detectors to have inverted. Therefore the absence of the peak is interpreted to mean that the level of irradiation of these pixels is likely to have been too low to cause inversion. Pixel 1 shows a slight peak at low voltages and so may have been just past the point of inversion. This explanation for the peaks absence is supported by depletion voltages (calculated in Section 4) which are estimated for these pixels to lie in the range 1 V below inversion to 12 V above inversion.

Measurements of the p-type detectors are discussed in Section 5.

3.2 Extraction of Damage Coefficients

To determine whether the measured leakage currents are consistent with expectations from known damage processes, damage coefficients were extracted for each structure and are tabulated in Table 3. The damage coefficient is given by

$$\alpha = \frac{\Delta I}{\Phi \cdot Vol}, \tag{2}$$

where Φ is the equivalent 1 MeV neutron fluence, Vol is the volume of the diode, and ΔI is the current increase due to irradiation. In determining ΔI, the initial current was neglected as it was more than 3 orders of magnitude lower than the final current. When calculating the damage coefficients, a uniform fluence across all structures was assumed with an equivalent 1 MeV neutron fluence of 4.8×10^{13} cm^{-2}.

The current used in calculating the damage coefficient was taken at the "Voltage Position" indicated in Table 3. For the n-type detectors the current was taken from the relatively flat portion to the right of the peak, or in cases where no flat region exists, the minimum to the right of the peak.

Fig. 10 shows the resulting damage coefficients for the n-type pixel arrays. The data points are presented with the x-axis locations in the same order left to right as the actual structures are on the boards. (See Fig. 1 for the pixel numbering.) The x-axis scale, however, is arbitrary, and the distance between the two detectors is greater than the distance between adjacent pixel arrays on the same detector. From this plot it is inferred that the beam intensity must have been increasing from left to right across detector "nam". Leakage current levels for pixels on detector "nar", which was to the right of detector "nam", were roughly uniform and similar to the leakage current levels of Pixels 3 and 6 of detector "nam", indicating that the beam profile was approximately flat in the region extending from the right of Pixels 3 and 6 of detector "nam".

We do not use the α value for the 450×75 μm^2 diode on detector "nar", since this structure had anomalously high currents compared to those in other structures nearby on the same detector. The cause of those currents is under investigation. An examination of the damage coefficients in Table 3 for all of the other n-type

Table 3 Damage coefficients based on a fluence of 4.8×10^{13} cm^{-2}. The column labeled "Voltage Position" indicates the voltage at which the current was extracted. The error on the current densities is estimated to be 5%.

Detector	Diode	Voltage Position (V)	Current (nA)	Diode Area (cm^2)	Current Density (μA/cm^{-2})	α (10^{-17} A/cm)
"nam"	1 mm^2	100	524	0.01	52	3.6
	330×330 μm^2	100	29.6	1.09×10^{-3}	27	1.9
	450×75 μm^2	100	10.7	3.38×10^{-4}	32	2.2
	Pix 1	100	2.68	2.68×10^{-4}	10	0.69
	Pix 2	100	6.17	2.68×10^{-4}	23	1.6
	Pix 3	150	14.3	2.68×10^{-4}	53	3.7
	Pix 4	100	2.56	2.68×10^{-4}	9.6	0.66
	Pix 5	100	6.30	2.68×10^{-4}	24	1.6
	Pix 6	150	14.8	2.68×10^{-4}	55	3.8
"nar"	1 mm^2	62	565	0.01	57	3.9
	330×330 μm^2	100	68.8	1.09×10^{-3}	63	4.4
	450×75 μm^2	100	27.6	3.38×10^{-4}	82	5.7
	Pix 1	150	16.2	2.68×10^{-4}	60	4.2
	Pix 2	150	14.5	2.68×10^{-4}	54	3.8
	Pix 3	150	13.7	2.68×10^{-4}	51	3.6
	Pix 4	150	16.4	2.68×10^{-4}	61	4.3
	Pix 5	150	15.4	2.68×10^{-4}	58	4.0
	Pix 6	150	14.6	2.68×10^{-4}	55	3.8

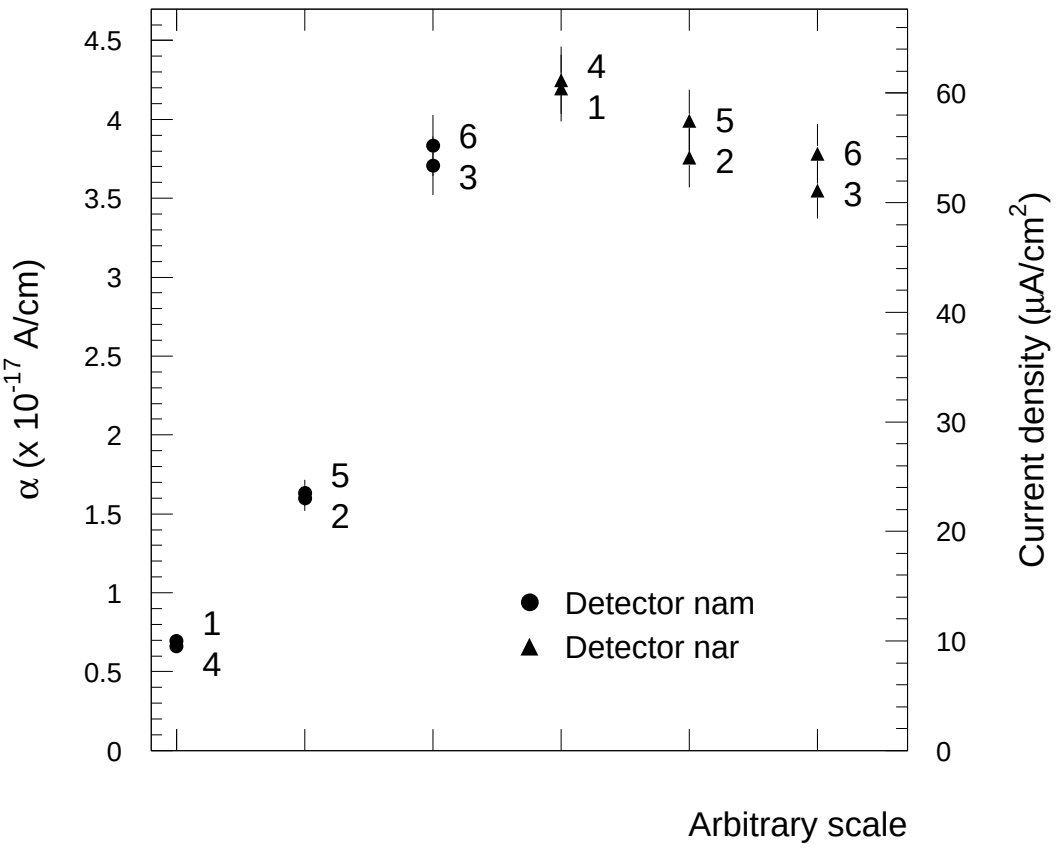

Figure 10: Damage coefficients α and current densities for the pixel arrays on detectors "nam" and "nar". The data are plotted so that the x positions are in the same order as the horizontal positions of the pixel arrays, but the distances are not to scale.

Table 4 Time intervals during which the detectors were at various temperatures. The actual time, the room temperature scaling factor $\theta(T)$, and the equivalent room temperature times are listed. The error on $\theta(T)$ was calculated using the error on E_I and an error of ± 1°C in the temperature. The error on the room temperature time is an estimate based on uncertainties in warm up times during transport.

Temperature (°C)	Actual Time	$\theta(T)$	Equiv. Time (days)
-17°C	15 months	0.002 ± 0.002	0.9 ± 0.9
0°C	50 days	0.04 ± 0.02	2 ± 1
20°C	2 ± 1 days	1	2 ± 1
Total			5 ± 2

structures shows that the maximum α is around $(3.6 - 4.4) \times 10^{-17}$ A/cm. This is a factor 2 higher than the damage coefficient for protons after complete annealing, $\alpha_{\infty,\mathrm{p}} = (2.22 \pm 0.10) \times 10^{-17}$ A/cm [3]. We conclude that this factor of 2 is due to incomplete annealing based upon an analysis explained in the text which follows.

3.3 Effects of Incomplete Annealing

To take into account the suppressed nature of annealing at low temperatures, a temperature-dependent scaling factor $\theta(T)$ for the time was used [3]:

$$\theta(T) = \exp\left(\frac{E_I}{k_B}\left[\frac{1}{293.2} - \frac{1}{T + 273.2}\right]\right) \tag{3}$$

where $E_I = 1.09 \pm 0.14$.

The equivalent room temperature intervals for the periods at different temperatures are calculated as the actual time multiplied by $\theta(T)$ and are given in Table 4. It is estimated that the detectors had a total of 5 ± 2 days of equivalent room temperature annealing.

The ratio $g(t)$ of the current after an annealing time t to the current immediately after an instantaneous irradiation can be parameterized as a sum of exponentials. Fig. 11 shows $g(t)$ obtained using annealing parameters from Ref. [6]. The expected ratio of the current after 5 ± 2 days of annealing to the current after complete annealing is given by:

$$\frac{g(5 \pm 2 \text{ days})}{g(t \to \infty)} = \frac{0.51 \pm 0.03}{0.30} = 1.7 \pm 0.1. \tag{4}$$

Therefore the damage coefficient after complete annealing is:

$$\begin{aligned} \alpha_\infty = \alpha(5 \pm 2 \text{ days}) \cdot \frac{g(t \to \infty)}{g(5 \pm 2 \text{ days})} &= \frac{(4.0 \pm 0.4) \times 10^{-17} \text{ A/cm}}{1.7 \pm 0.1} \\ &= (2.4 \pm 0.3) \times 10^{-17} \text{ A/cm}. \end{aligned} \tag{5}$$

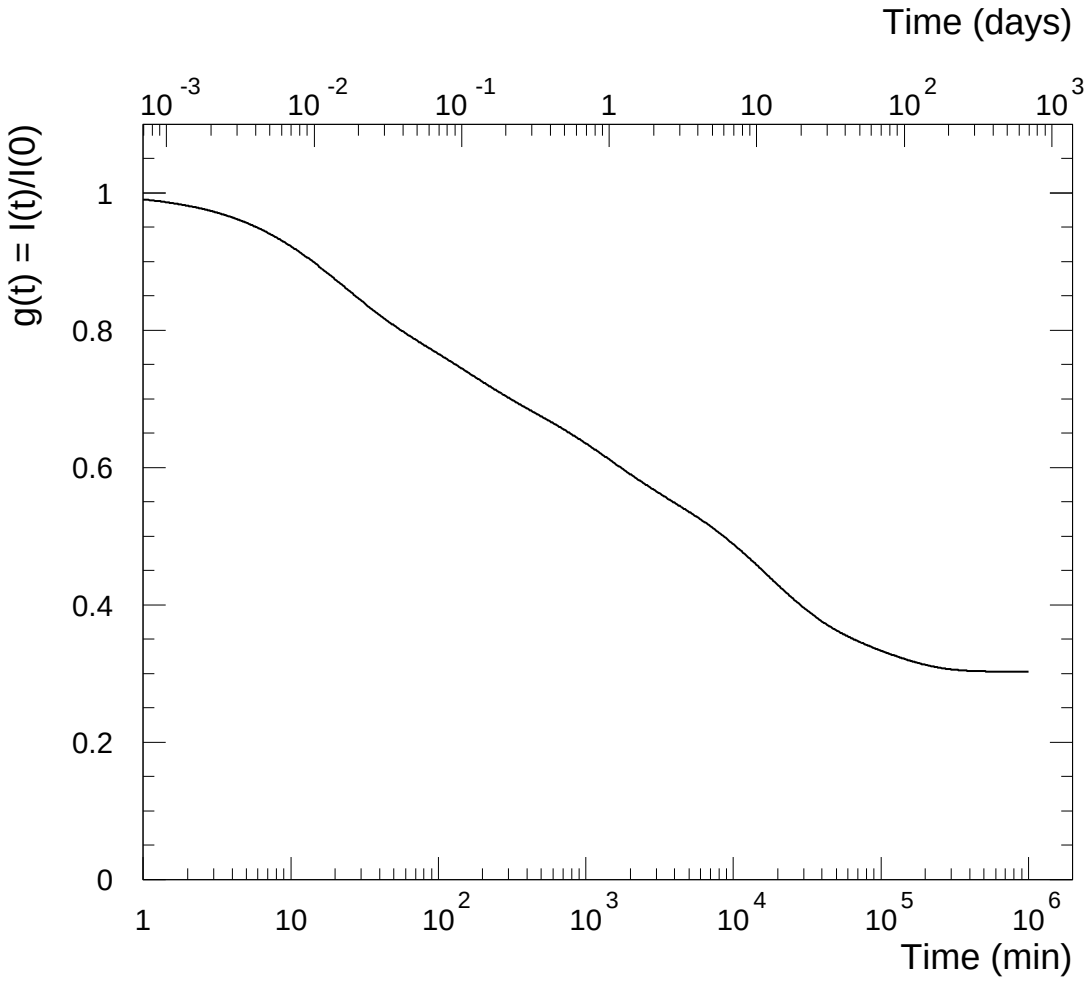

Figure 11: Ratio $g(t)$ of the current after a room temperature annealing time t to the current immediately after an instantaneous irradiation, versus time. The plot was produced using annealing parameters from Ref. [6].

Table 5 Position of peaks from I-Vs of detectors "nam" and "nar". Fluences Φ' are calculated by normalizing Pix 4 of detector "nar" to a fluence 4.8×10^{13} cm^{-2} and scaling with respect to current densities. Depletion voltage was calculated based on these fluences and was not measured directly. The upper and lower limits were calculated by using the extremes of the parameters involved and so are effectively added linearly. Positive values for the depletion voltage indicate that the detector has inverted.

Detector	Diode	Peak Position (V)	Current Density (μA/cm^{-2})	Fluence Φ' (10^{13} cm^{-2})	V_{dep} (V)
"nam"	Pix 1	–	10	0.8	6 ± 6
	Pix 2	7.8	23	1.8	26 ± 8
	Pix 3	24	53	4.2	52 ± 10
	Pix 4	–	9.6	0.7	5 ± 6
	Pix 5	11	24	1.8	26 ± 8
	Pix 6	36	55	4.3	53 ± 10
"nar"	Pix 1	32	60	4.7	57 ± 10
	Pix 2	20	54	4.2	52 ± 10
	Pix 3	21	51	4.0	50 ± 10
	Pix 4	30	61	4.8	57 ± 10
	Pix 5	32	58	4.5	55 ± 10
	Pix 6	35	55	4.3	52 ± 10

The error on the above damage coefficient is completely due to errors in the annealing correction and the spread in damage coefficients. The error in the fluence is not well known and could be as high as 50%.

We conclude from the result expressed in Eq. (5) that the observed leakage currents are consistent with expectations from known damage and annealing processes.

3.4 Extraction of the Fluence Profile from Leakage Current Information

Uncertainties in the current densities in Table 3 are sufficiently small that variations in the central values can be used to recover the profile of the beam that caused the damage. We assume that the maximum current density in the pixel arrays, 61 μA/cm^2, (which occurs in Pixel 4 of detector "nar") corresponds to the maximum fluence, 4.8×10^{13} cm^{-2}. We then scale the current densities of the remaining pixels by $4.8 \times 10^{13}/61$ and predict the fluences at these pixel locations. The resulting fluences are given in Table 5 and shown graphically in Fig. 12a.

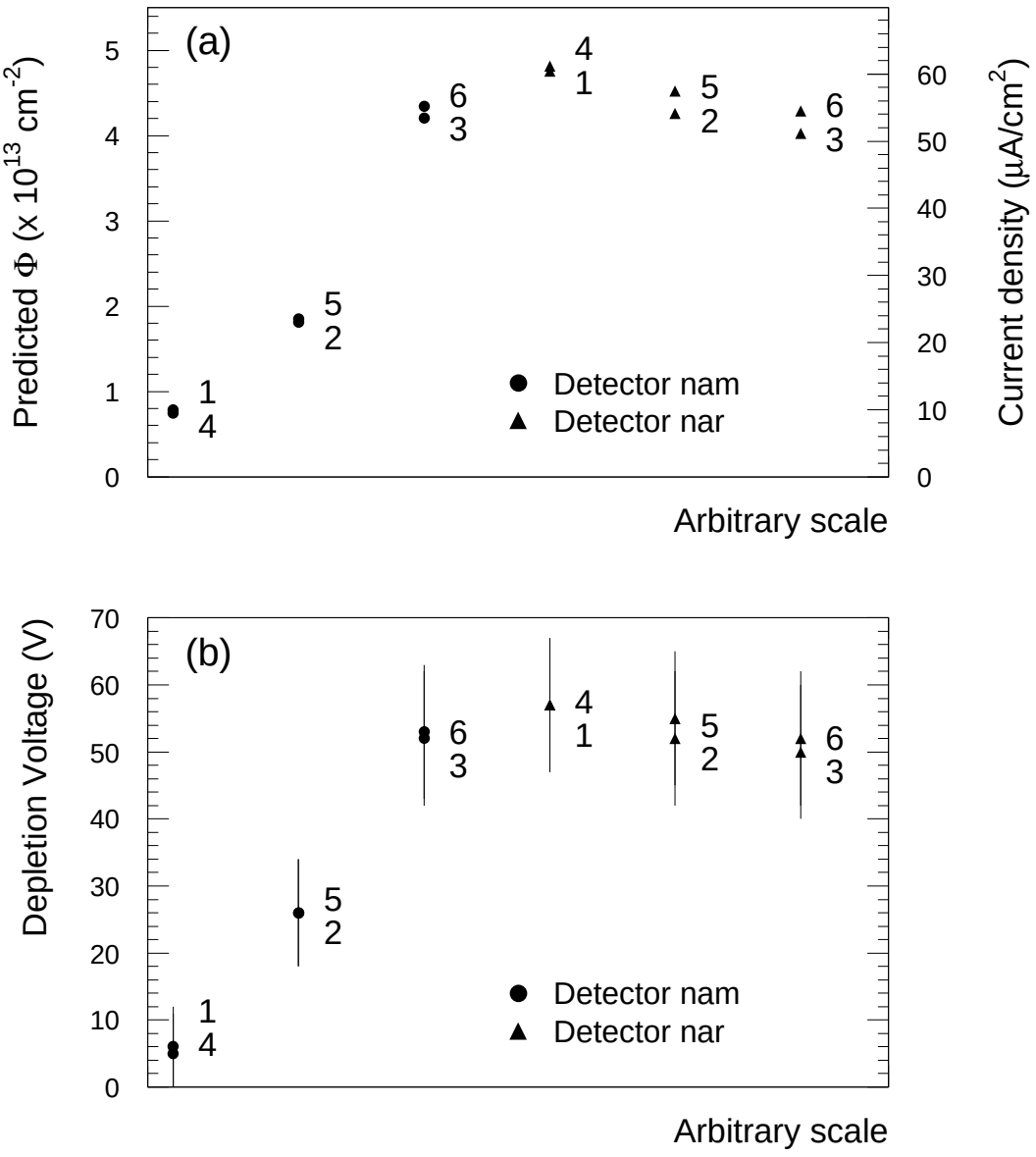

Figure 12: (a) Predicted fluences based on variations in the current density of the pixel arrays. Fluences are normalized to 4.8×10^{13} cm^{-2} for a current density of 61 μA/cm^2. (b) Depletion voltages calculated (see text) using the fluences shown in (a).

4 Depletion Voltage Results of n-type Detectors

4.1 Depletion Voltages of Unirradiated Detectors

Bulk capacitance versus voltage ("C-V") was measured using a Keithley 237 as the bias supply and a HP4284A LCR meter to measure the capacitance. Fig. 13 shows a C-V for one of the relatively large unirradiated n-type diodes. The size of the structure allows us to apply a parallel plate capacitor approximation to the geometry to extract the depletion voltage. The extracted depletion voltage was 20 V with a corresponding effective doping density of 2.9×10^{11} cm^{-3}. Fig. 14 shows a C-V for a similar size unirradiated p-type diode. The depletion voltage was 80 V with a corresponding effective doping density of 1.2×10^{12} cm^{-3}.

4.2 Calculation of Depletion Voltages of Irradiated Pixels

The small area of the pixels makes extraction of their depletion voltage from C-V measurements inappropriate. Instead the following calculation was used to obtain depletion voltages of irradiated pixels by estimating the fluence and using published results of the fluence dependence of the depletion voltage.

The effective doping density as a function of fluence is expected to be

$$N_{\text{eff}}(\Phi) = N_{\text{eff},0} - N_{\text{C0}}(1 - e^{-c\Phi}) - g_C\Phi - g_Y\Phi\left(1 - \frac{1}{1 + g_Y\Phi k(T)t}\right) \qquad (6)$$

where Φ is the equivalent 1 MeV neutron fluence, t is the time after irradiation, and $N_{\text{eff},0}$ is the initial effective doping density (positive for n-type material) as calculated in Section 4.1. Values for the other parameters are given in Table 6. The last term in Eq. (6) is due to reverse annealing; its rate is dependent on the temperature and fluence. The temperature dependence of k is given by

$$k(T) = k_{293.15}\ \exp\left(\frac{E_a}{k_B}\left[\frac{1}{293.15} - \frac{1}{T}\right]\right). \qquad (7)$$

Values for E_a and $k_{293.15}$ are also given in Table 6. There is some correlation between $k_{293.15}$ and E_a, but it is sufficiently weak that they can be treated as uncorrelated parameters with negligible impact on the overall error of N_{eff}. The parameters in Table 6 may be used if all short term annealing has completed. This is appropriate for the measurements here since most of the short term annealing occurs within a few weeks even at 0°C.

The depletion voltage V_{dep} is proportional to N_{eff}:

$$V_{\text{dep}} = \frac{|N_{\text{eff}}|qd^2}{2\epsilon_{\text{Si}}}, \qquad (8)$$

where q is the electron charge, d is the detector thickness, and ϵ_{Si} is the permittivity of silicon.

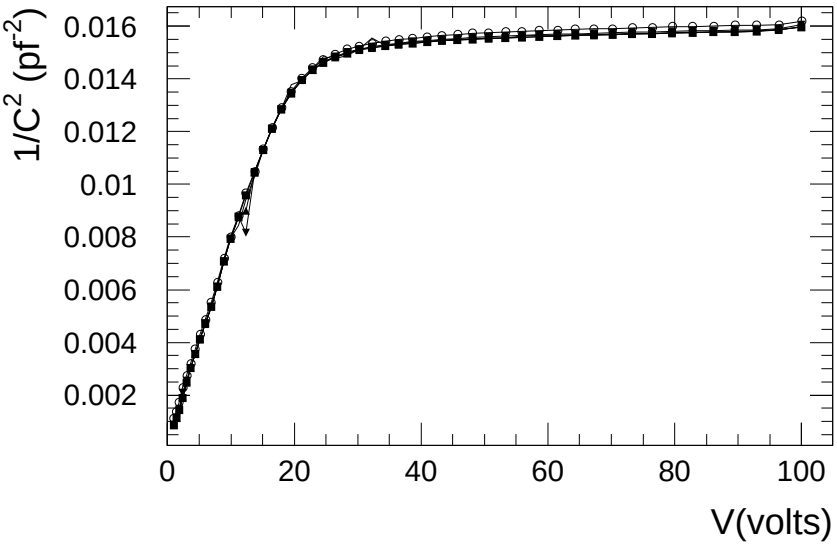

Figure 13: Bulk capacitance versus bias voltage of an unirradiated 6.7×3.2 mm^2 n-type diode. Multiple curves reflect measurements made at several frequencies ranging from 1 kHz to 1 MHz.

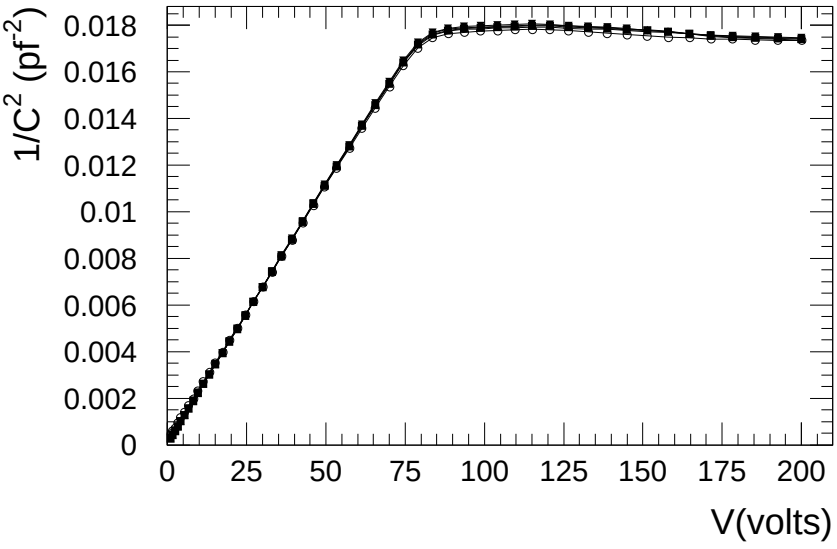

Figure 14: Bulk capacitance versus bias of an unirradiated 6.7×3.2 mm^2 p-type diode. Multiple curves reflect measurements made at several frequencies ranging from 1 kHz to 1 MHz.

Table 6 Parameters used in Eq. (6) for the fluence dependence of effective doping density. Parameters are taken from Ref. [3] and are appropriate for protons. The error on $k_{293.15}$ was calculated from parameters in Ref. [3] along with the appropriate covariance matrix [7]. A range is given for N_{C0} as it is strongly dependent on the starting material.

Parameter	Value
g_Y (10^{-2} cm^{-1})	5.8 ± 0.3
g_C (10^{-2} cm^{-1})	1.15 ± 0.09
N_{C0} (10^{11} cm^{-3})	5.47 (4.08 to 6.85)
c (10^{-13} cm^2)	0.96 ± 0.19
E_a (eV)	1.31 ± 0.04
$k_{293.15}$ (10^{-20} cm^3/s)	1.55 ± 0.21

Uncertainties in the annealing time and temperature (relevant to the reverse annealing) were incorporated using a similar method to that used in Section 3.3, except that E_I was replaced with E_a in Eq. (3). This resulted in an equivalent room temperature reverse annealing time of $t = (3.4 \pm 1.1)$ days. Eq. (6) was then used with this value of the time and $k(T) = k_{293.15}$.

Fig. 15 shows a plot of N_{eff} as a function of fluence. The $\pm 1\ \sigma$ limits are shown which were calculated using error propagation. Most of the uncertainty is in N_{C0}, which depends strongly on the starting material used.

The expected depletion voltages were calculated using Eqs. (6) and (8) with the fluences listed in Table 5, which were obtained by scaling the leakage currents. The calculated depletion voltages for the pixel arrays are included in Table 5 and are plotted in Fig. 12b.

Without reverse annealing the depletion voltage is reduced by about 2% for a fluence of 2×10^{13} cm^{-2} and by about 6% for a fluence of 5×10^{13} cm^{-2}.

The mean values of the depletion voltages calculated this way are about 15–30 V beyond the position of the peaks in the I-V curves of Figs. 4 and 6. This would be consistent with the detectors reaching full depletion somewhere on the right-hand tail of each peak.

5 Measurements of p-type Detectors

5.1 Leakage Currents of Irradiated and Unirradiated Detectors

Leakage currents in unirradiated p-type detectors are shown in Figs. 16 and 17. The currents were low (on the order of 2 pA) and consequently difficult to measure. The I-V shapes are not always consistent with that expected for a reverse-biased diode.

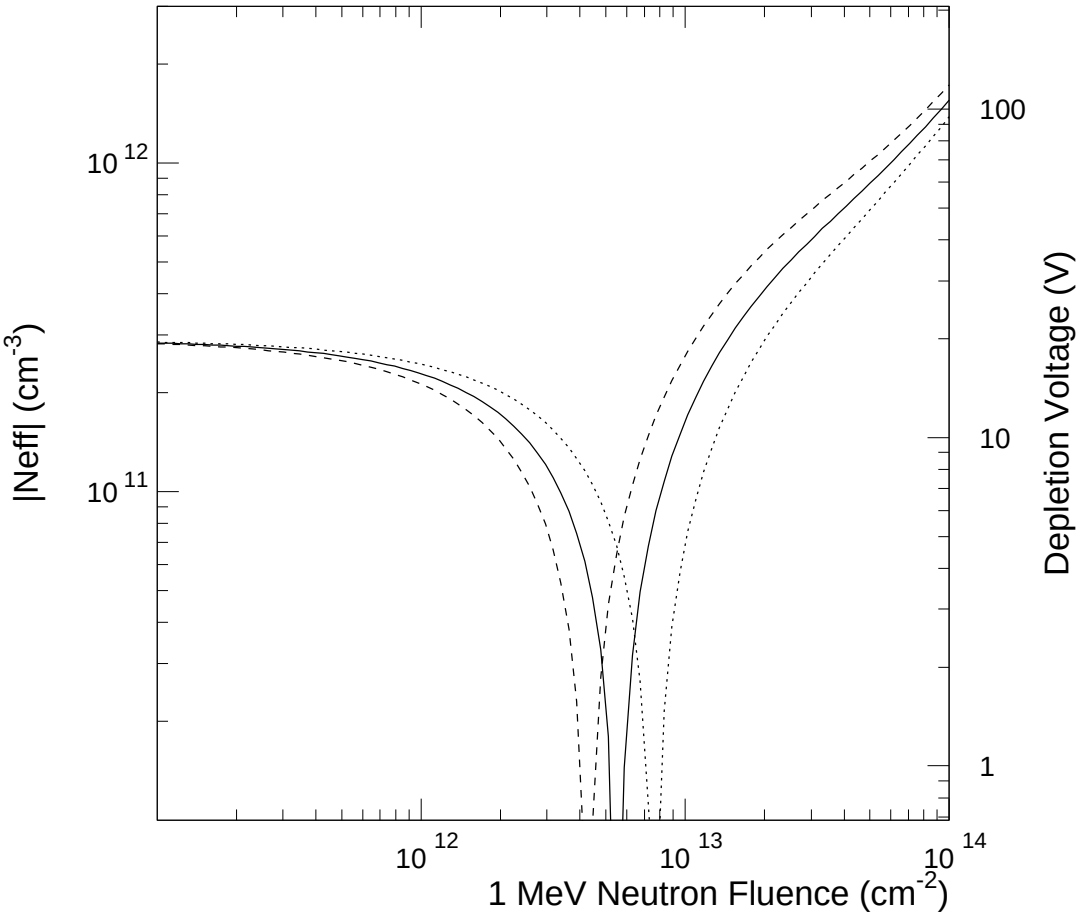

Figure 15: Effective doping density and depletion voltage as a function of equivalent 1 MeV neutron fluence. The solid line is calculated using the mean values of parameters in Table 6. The ± 1 σ limits are shown by the dashed and dotted lines.

Table 7 Damage coefficients based on a fluence of 4.8×10^{13} cm^{-2} for structures on the p-type detectors "pcm". The I-V curve was extrapolated (see text) to the expected depletion voltage as indicated in the column labeled "Voltage Position". The three voltage values reflect the uncertainty in the depletion voltage (159 ± 10 V).

Diode	Voltage Position (V)	Current (μA)	Diode Area (cm^2)	Current Density (μA/cm^{-2})	α (10^{-17} A/cm)
2 mm^2	149	1.51	0.02	75	5.2
	159	1.56	0.02	78	5.4
	169	1.61	0.02	81	5.6
1 mm^2	149	0.60	0.01	60	4.2
	159	0.62	0.01	62	4.3
	169	0.64	0.01	64	4.4

For example, Pixel 5 has a spike at zero volts for some runs and not for others. Pixel 1 shows a sign change in its current and has current levels more than 3 orders of magnitude higher than the other pixel arrays. Some anomalies are not too surprising since at such low levels contributions from surface currents are significant. Pixel array 1 has no p-stops; its behavior may indicate that the p-stops are indeed necessary.

I-Vs for the irradiated p-type structures are shown in Fig. 18. The p-type detectors show a steady increase in the current with voltage before breaking down around 80 V.

Assuming the procedure for calculating depletion voltages as described in Section 4 is valid for p-type detectors, the expected depletion voltage for a fluence of 4.8×10^{13} cm^{-2} is 159 ± 10 V (given an initial depletion voltage of 80 V). The detectors, therefore, are breaking down before they are fully depleted.

Since the detectors are breaking down before they fully deplete, it is difficult to know what current to use for calculating the damage coefficients. The current that would have been reached at full depletion in the absence of breakdown was predicted by extrapolating the data in a plot of current versus (voltage)$^{1/2}$ to the expected depletion voltage. The resulting currents and damage coefficients are given in Table 7.

The damage coefficients (before correction for annealing) for the 1 mm^2 and 2 mm^2 p-type diodes are $(4.3 \pm 0.1) \times 10^{-17}$ and $(5.4 \pm 0.2) \times 10^{-17}$ A/cm respectively. Assuming the annealing rate is the same for p-type as it is for n-type material, these damage coefficients can be divided by a factor of 1.7 ± 0.1 (see Section 3.3) to obtain the damage coefficient after complete annealing. The α for the 1 mm^2 diode is consistent within errors with α obtained for n-type detectors, while the α for the 2 mm^2 diode is 35% higher. Additional measurements of p-type structures are underway in an effort to shed further light upon their leakage current properties.

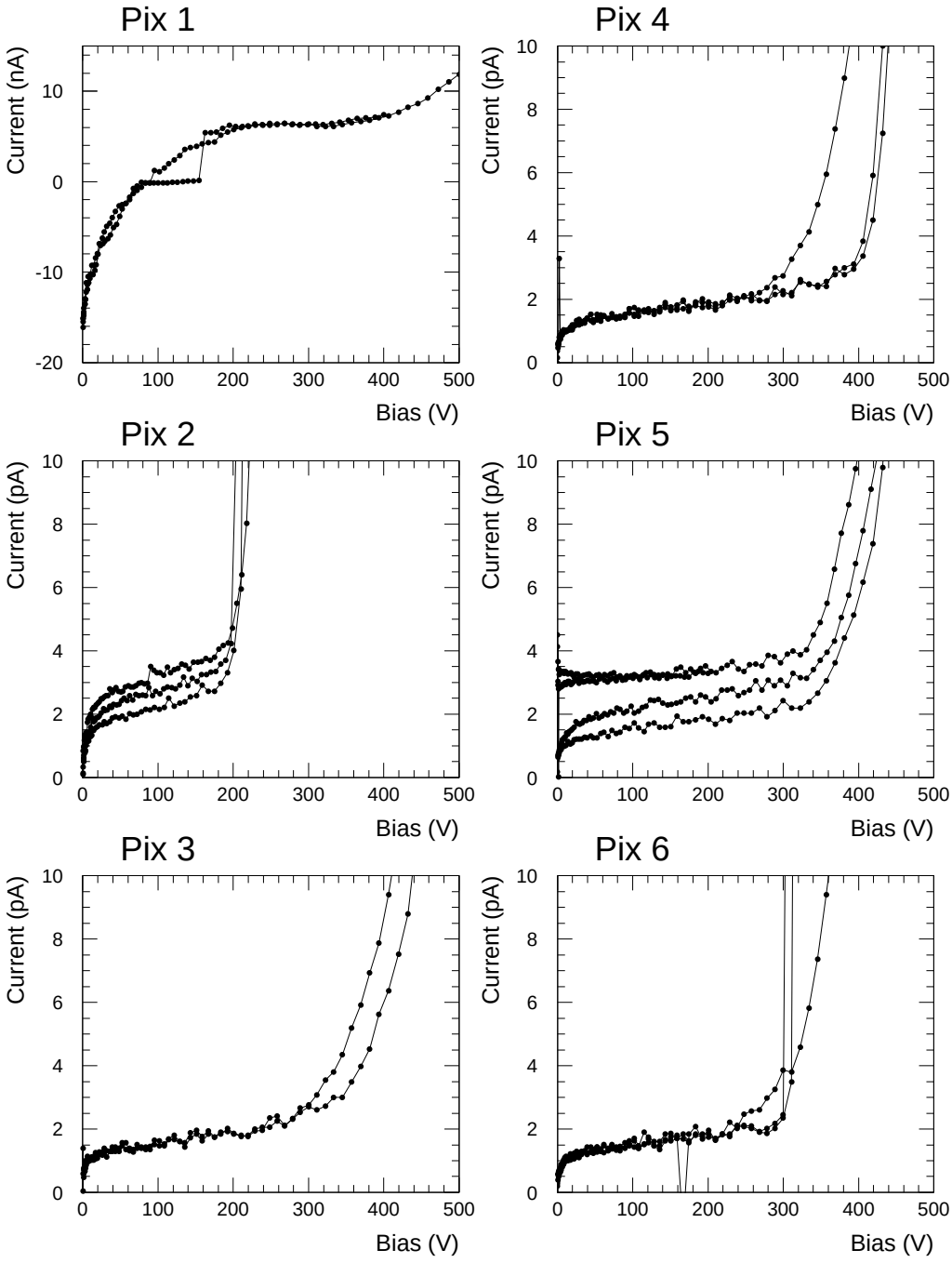

Figure 16: Currents in p-type pixel arrays on detector "p1". This detector was unirradiated. Currents were temperature corrected to 20°C. Multiple curves reflect repeated measurements.

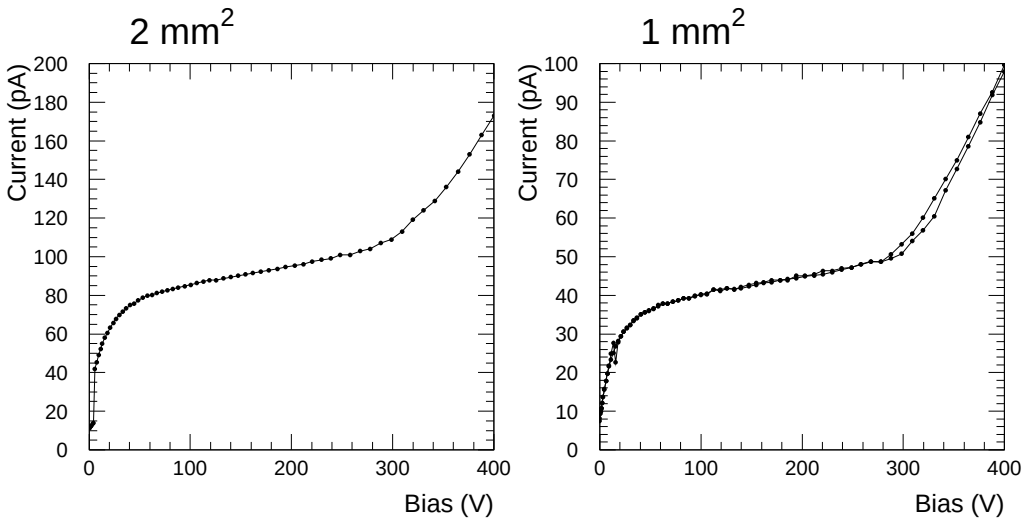

Figure 17: Currents in non-pixel structures on the p-type detector, "p1". This detector was unirradiated. Currents were temperature corrected to 20°C.

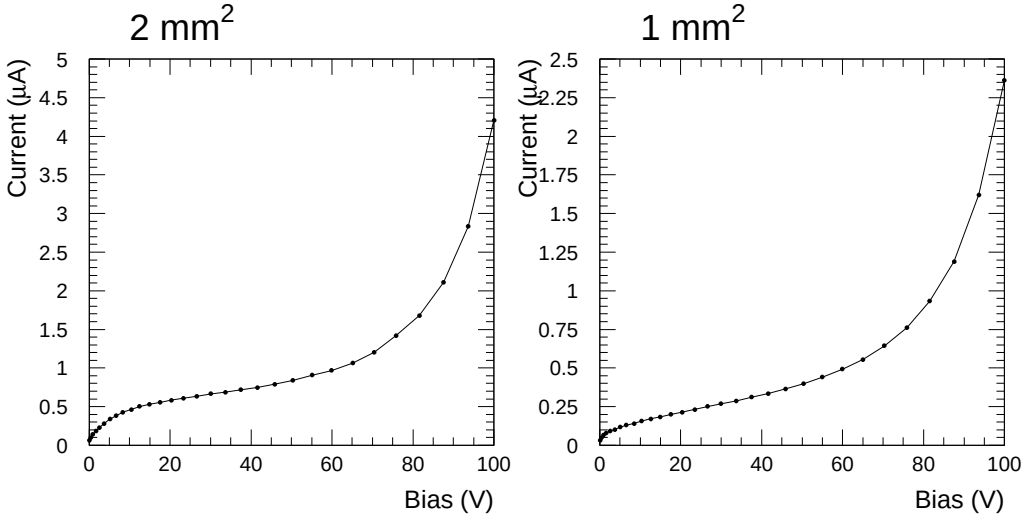

Figure 18: Currents in p-type structures on detector "pcm". Currents were temperature corrected to 20°C. Multiple curves reflect repeated measurements.

5.2 Breakdown Voltages

The breakdown voltages of diodes on the unirradiated p-type detector "p1" (see Figs. 16 and 17) were around 300 V. The same type structures after irradiation (Fig. 18) have breakdown voltages which are much lower, around 80 V. This result could have a profound influence on the choice of substrate for ATLAS pixel sensors. Please see the extensive discussion in the companion note to this one. [8]

6 Conclusions

Leakage currents measured on n-type pixels irradiated with an equivalent of 4.8×10^{13} cm^{-2} 1 MeV neutrons predict a damage coefficient after complete annealing of $(2.4 \pm 0.3) \times 10^{-17}$ A/cm, which is consistent with published values [3]. We consequently conclude that the current is being produced by mechanisms explained by existing theories of radiation damage and annealing. It should be noted, however, that there is some uncertainty in the fluence which is not included in the error presented.

Measurements of two similarly damaged p-type structures resulted in a damage coefficient for one structure being consistent with the α obtained for n-type detectors and a damage coefficient for the other which is 35% higher. Further investigations of these structures and similar ones are in progress.

The leakage currents for irradiated n-type detectors which received sufficient fluence to cause inversion of the bulk to p-type peak at a position correlated with the depletion voltage. If p^+ on n-type bulk detectors are used in ATLAS, the peak could be a problem as it will increase the current levels during voltage ramp-up beyond that calculated with known damage coefficients. Also, since the depletion voltage increases with irradiation, the peak is expected to broaden — if detectors are operated below full depletion, they may be operating in the region of the peak.

In p-type detectors, significant diminishment of the breakdown voltage with irradiation was observed. This highlights the importance of the need for careful design of detectors for ATLAS.

7 Acknowledgments

We would like to thank M. Gilchriese for his interest in this work and for useful discussions. We are also grateful for the assistance of T. Collins and M. Hoeferkamp. This work was supported in part by grant PHY-9508459 from the National Science Foundation.

References

[1] A. Van Ginneken, *Non Ionizing Energy Deposition in Silicon for Radiation Damage Studies,* FERMILAB report FN-522 (1989).

[2] Annual Book of ASTM Standards, Vol 12.02, chap. ASTM E722-85, (1985) p. 324.

[3] A. Chilingarov, H. Feick, E. Fretwurst, G. Lindström, S. Roe, T. Schulz, *Radiation Studies and Operational Projections for Silicon in the ATLAS Inner Detector*, Nucl. Instr. and Meth. A 360 (1995) 432.

[4] P. Fischer, *et al.*, *Pixel Detector Back-up Document to Support the ATLAS Technical Proposal*, ATLAS Internal Note INDET-NO-086 (1994).

[5] A. Brandl, *et al.*, *Measurement of Proton-Induced Radiation Damage Effects in Double-Sided Silicon Microstrip Detectors*, CDF Collaboration Internal Note CDF/DOC/SEC_VTX/PUBLIC/3512, in preparation.

[6] R. Wunstorf, Ph.D. thesis, Universität Hamburg (1992).

[7] Henning Feick, Universität Hamburg, private communication

[8] G. Gorfine and S. Seidel, *Measurement and Simulation of Electrical Breakdown in p-type Silicon Sensors*, ATLAS INDET note in preparation.